

Recent Progress in Reducing the Uncertainty in and Improving Pyranometer Calibrations

Daryl R. Myers

e-mail: daryl_myers@nrel.gov

Thomas L. Stoffel

Ibrahim Reda

Stephen M. Wilcox

Afshin M. Andreas

National Renewable Energy Laboratory,
Distributed Energy Resources Center,
1617 Cole Blvd.,
Golden, CO 80401

The Measurements and Instrumentation Team within the Distributed Energy Resources Center at the National Renewable Energy Laboratory, NREL, calibrates pyranometers for outdoor testing solar energy conversion systems. The team also supports climate change research programs. These activities led NREL to improve pyranometer calibrations. Low thermal-offset radiometers measuring the sky diffuse component of the reference solar irradiance removes bias errors on the order of 20 Watts per square meter (W/m^2) in the calibration reference irradiance. Zenith angle dependent corrections to responsivities of pyranometers removes 15 to 30 W/m^2 bias errors from field measurements. Detailed uncertainty analysis of our outdoor calibration process shows a 20% reduction in the uncertainty in the responsivity of pyranometers. These improvements affect photovoltaic module and array performance characterization, assessment of solar resources for design, sizing, and deployment of solar renewable energy systems, and ground-based validation of satellite-derived solar radiation fluxes. [DOI: 10.1115/1.1434262]

Introduction

Assessing solar resources for design and deployment of renewable energy systems; evaluating photovoltaic (PV) cell, module, and array performance; ground-based validation of satellite-derived solar radiation fluxes; and climate change issues all rely on the accurate radiometer calibrations. Pyrheliometers (Fig. 1) measure shortwave (300 nanometer [nm] to 2500 nm wavelength) solar radiation direct-beam radiation within a 5 deg field of view around the solar disk.

Pyranometers (Fig. 2) measure the total shortwave global or hemispherical solar radiation, to characterize performance of flat-plate PV technologies. Pyrheliometer measurements are important for concentrating solar collector technologies.

Solar Radiometer Calibrations

The ratio between the radiometer output signal (microvolts) and solar power flux, or irradiance, (W/m^2) is the radiometer calibration factor. NREL's Broadband Outdoor Radiometer Calibration (BORCAL) procedures characterize and calibrate pyrheliometers and pyranometers. Our new procedures improve our Radiometric Calibration (RADCAL) techniques [1–4]. Our Radiometer Calibration and Characterization (RCC) software implements BORCAL data collection, reporting, and data archiving [5].

The NREL team has worked with the U.S. Department of Energy (DOE) Atmospheric Radiation Measurement Program (ARM), National Aeronautics and Space Administration (NASA) Earth Observing System (EOS) Validation Program, World Meteorological Organization (WMO) Baseline Surface Measurement Network (BSRN), and National Oceanic and Atmospheric Administration (NOAA) Climate Monitoring and Diagnostics Laboratory (CMDL) to identify, characterize, and reduce sources of error and uncertainty in broadband shortwave radiation calibrations and measurements [6–10].

Contributed by the Solar Energy Division of the American Society of Mechanical Engineers for publication in the ASME JOURNAL OF SOLAR ENERGY ENGINEERING. Manuscript received by the ASME Solar Energy Division, October 2001; final revision April 2001. Associate Editor: S. Kleis.

1 Broadband Outdoor Radiometer Calibrations (BORCAL).

1.1 The BORCAL Reference Irradiance. The WMO World Radiometric Reference (WRR) is the foundation of NREL's BORCAL procedures. The WRR is the international reference for mea-



Fig. 1 Pyrheliometers measuring direct-normal solar radiation

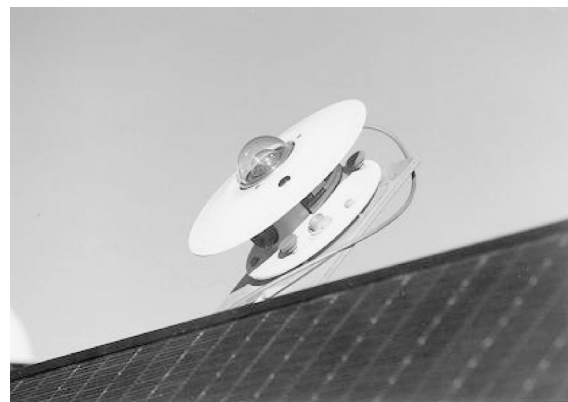


Fig. 2 Pyranometer measuring total global hemispherical radiation

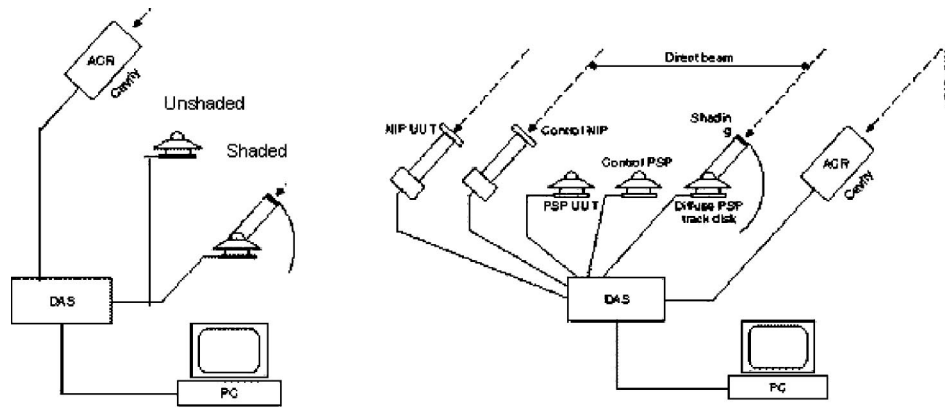


Fig. 3 Shade/Unshade and component summation calibrations

asuring the direct-beam solar irradiance using absolute-cavity pyrheliometers [11–14]. Transfer of a WRR-traceable calibration to field pyrheliometers is by direct comparison between an absolute-cavity pyrheliometer and the pyrheliometer [13–15]. Transfer of a WRR traceable calibration to field pyranometers can be done using an absolute-cavity pyrheliometer and a shade/unshade procedure for the test pyranometers [13,15]. Alternatively, a reference irradiance from an absolute-cavity pyrheliometer direct-beam measurement and a diffuse-sky radiation measurement can be computed (*component summation* method). Here, the diffuse-sky radiation must be measured with a pyranometer under a sun-tracking shading disk that blocks the same solid angle as the field of view of the cavity pyrheliometer.

1.2 Calibration Techniques. Figure 3 is a schematic of the shade/unshade and component summation techniques, respectively. For the shade/unshade protocol, the responsivity, R_s , is the ratio of the pyranometer signal to the input signal induced by the vertical component of the direct beam, $I_{dn} \times \cos(z)$, where z is the zenith angle. Shading the pyranometer with a disk subtending the same solid angle as the field of view of a cavity pyrheliometer produces a signal, V_s . The unshaded signal is V_u , and the responsivity is computed as:

$$R_s = (V_u - V_s) / (I_{dn} * \cos(z)) \quad (1)$$

Procedures for acquiring shade/unshade calibration data are described in the American Society for Testing and Materials Standard E-913 [18]. The measurement and timing sequence for the shade/unshade approach is shown in Fig. 4.

Time period A is a 30-minute stabilization period. Time period B is 20 to 30 time constants ($1/e$, or 63% of final steady-state

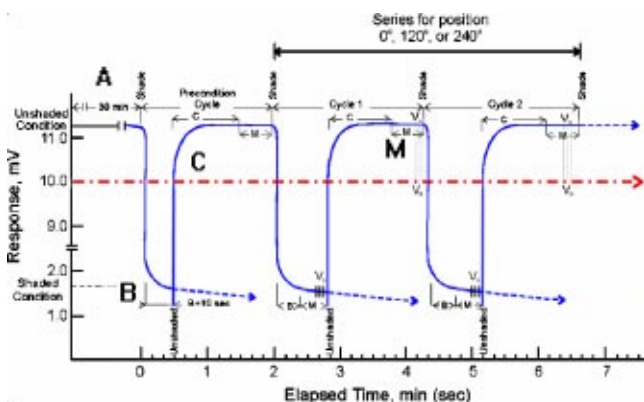


Fig. 4 ASTM sequence for shade/unshade calibration procedures

values) for the instrument response. Period C is 60 time constants for the instrument response. These periods were chosen to reduce the influence of possible multiple time constants known to exist [19]. During period M at least three readings of instrument response, V_s or V_u , and the direct-beam irradiance, are recorded. The mean zenith angle and cavity pyrheliometer data during the measurement periods M are used in computing the $I_{dn} \times \cos(z)$ terms. A sufficient number of R_s versus Z are required to map out the cosine response of the radiometer. For the *component summation* technique, a pyranometer is continuously shaded by a tracking shading disk to measure the diffuse-sky irradiance, as shown in Fig. 5. The pyranometer(s) used under the tracking shading disk must first be calibrated using the shade/unshade technique. Whether ventilated (which may reduce, but not eliminate thermal offsets, described below) or unventilated, the calibration is valid only for the same configuration in the application of the instrument.

1.3 Diffuse Radiometer Calibration. The first improvement implemented in the our procedures is to determine the responsivity of the diffuse reference pyranometer as the mean of the respon-



Fig. 5 Tracking shading disks for pyranometer measurement of diffuse-sky radiation

sivities in three azimuthal directions (0 deg [south], 120 deg, and 240 deg) at $Z=45$ deg, representing an *average zenith angle* for clear sky diffuse radiation. Azimuthal variations in responsivity of 1.5% are smoothed using the mean. Our analysis results in a total uncertainty of 2.5% of reading in the clear sky diffuse-sky irradiance (I_{df}), and 6.5% of reading under variable sky conditions, if all other sources of uncertainty (data loggers, environmental conditions, etc.) are accounted for [8,20].

1.4 Component Summation and Diffuse Thermal Offsets. Our next improvement was to recognize the negative bias error introduced by all-black sensor pyranometers measuring diffuse sky radiation, and replace them with black-and-white sensors. In the component summation approach, the global reference irradiance is the sum $I_{dn} \times \cos(z)$ and the diffuse-sky radiation, I_{df} . Individual pyranometer signals, V_u , are divided by the reference irradiance to produce the individual pyranometer responsivity:

$$Rs = Vu / (I_{dn} * \cos(z) + I_{df}) \quad (2)$$

Research within the DOE ARM program, NASA EOS Validation Program, WMO BSRN, and NOAA CMDL revealed thermal offset, W_{off} (W/m^2), bias errors in both calibration techniques not accounted for in the previous analysis. This offset appears in all-black thermopile pyranometers without compensating thermopiles, such as the Eppley Precision Spectral Pyranometer, (PSP), and is site dependent [6,21]. The offset is a negative bias error in addition to the 2.5% uncertainty in the responsivity. Clear sky W_{off} for the NREL site has been characterized to be $15 W/m^2$ ($\pm 5 W/m^2$, 2 standard deviations) throughout the year; as described below.

Thermopile-based pyranometers rely on the temperature difference between junctions of dissimilar metals in contact with a surface that absorbs solar radiation (*hot junctions*) and reference, or *cold junctions*, that do not receive any solar radiation. In Fig. 6, the top unit, an Eppley Laboratory Model PSP is an example of these *all-black* sensor pyranometers. Another type of thermopile has the hot junctions in contact with a black absorbing surface and the reference cold junctions under a white surface that absorbs



Fig. 6 All-black (top unit) and black-and-white thermopile pyranometers under tracking shading disks

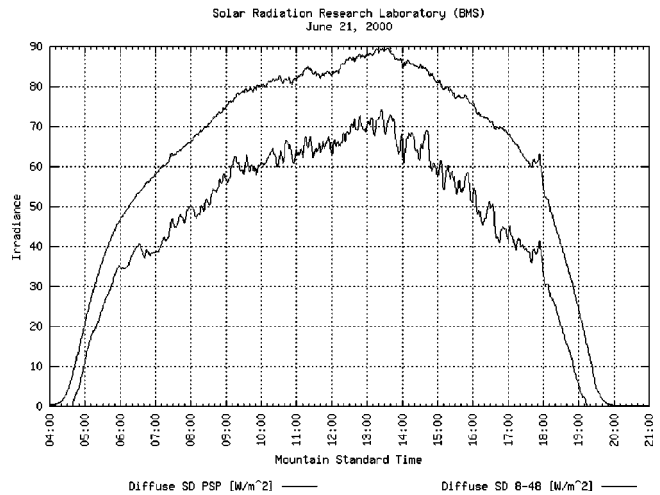


Fig. 7 Black-and-White (top line) and all-black sensor clear sky diffuse irradiance demonstrating 20 W/m^2 thermal offset in all-black pyranometer

very little shortwave solar radiation. The bottom instrument in Fig. 6 is an example of the latter, an Eppley Laboratory Model 8–48 *black-and-white* unit.

Pyranometers with all-black receivers are rarely in thermal equilibrium when deployed outdoors. Thermal infrared (IR) energy is exchanged among the absorbing sensor, dome, and sky. These exchanges result in a net negative thermal offset, W_{off} , in the thermopile voltage signal. Black-and-white pyranometer thermal offsets are smaller as all junctions see the same thermal radiation. Figure 7 is an example plot of all-black (PSP) detector (lower line) and a black-and-white detector (upper line) clear-sky diffuse irradiance at NREL. Both radiometers were calibrated in the same RCC event, using the new procedures. We computed the mean difference in clear sky shading disk diffuse data from both radiometers over a 6-month period (January to July, over 70,000 1-minute samples) to be $15 W/m^2 \pm 5 W/m^2$, (expanded uncertainty, 2 standard deviations). The W_{off} for the black-and-white units has been experimentally determined (by repeated shading outdoors) to be about $2 W/m^2$.

Radiometer Characterization and Calibration (RCC)

In 2000, we revised the RCC software and hardware to address diffuse pyranometer azimuthal response, thermal offsets in all-black pyranometer detectors, and improvements in computation of zenith angles. Uncertainty analysis of our revised procedures shows reduced uncertainty in our BORCAL process. This section describes the technical improvements in determining pyranometer responsivities.

1 RCC Configuration and Operation. RCC software requires rigorous configuration and setup session all equipment. In addition to the reference (direct and diffuse) and test (pyranometer, pyrhemometer) sensors, RCC requires *control* instruments included in every calibration to monitor the process stability. Silicon photodiode atmospheric stability radiometer (ASR) units measure irradiance stability. Instability is reported by flagging the data and alerting the operator. Meteorological data for temperature and relative humidity are recorded. Rather than require the additional expense of calibrating a sunphotometer and measuring turbidity, the software estimates an *equivalent broadband turbidity* [22] using the direct normal irradiance and algorithms derived at NREL [23,24]. Various conditions set alarms and flag suspect data. These include:

- Mismatch of more than 18% between ASR and Reference irradiances.

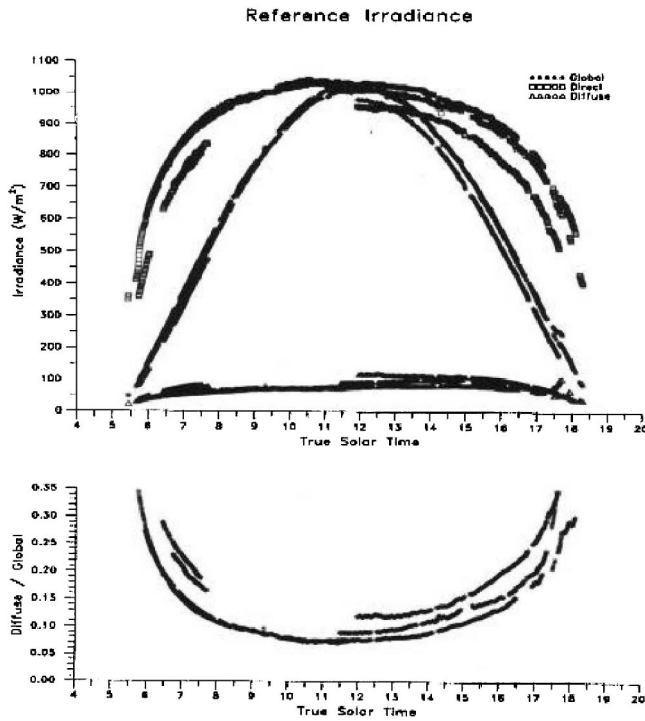


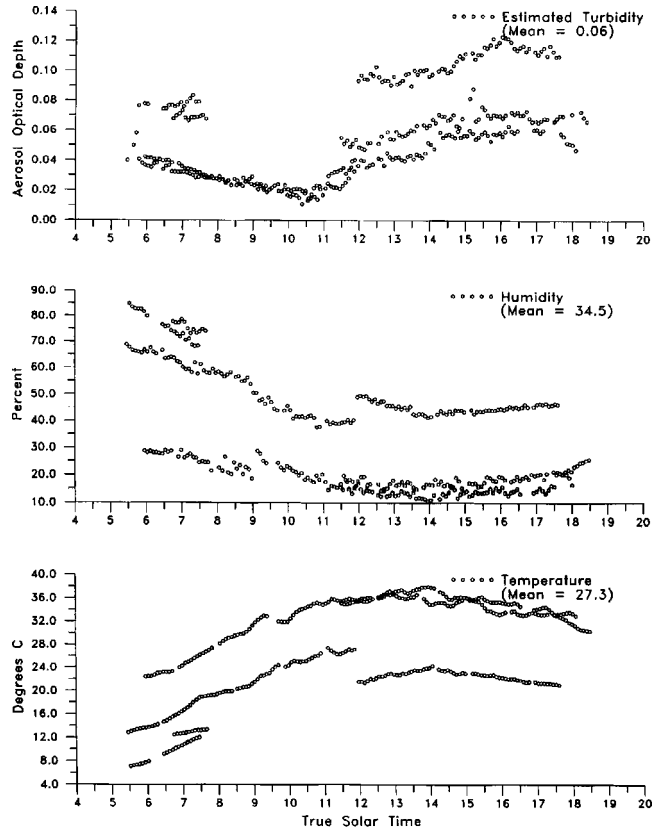
Fig. 8 Reference global, direct, and diffuse components (top); Ratio of diffuse-sky irradiance to total global reference irradiance (bottom)

- Mismatch between multiple reference instruments (1% between multiple cavity radiometers, or 6% between two diffuse pyranometers).
- Difference $>0.5\%$ between adjacent responsivities for a single instrument.
- Mismatch $>6\%$ between the reference irradiance and a control instrument
- A difference between adjacent readings of meteorological instruments $>3^\circ\text{C}$ for temperature, or $>7\%$ in relative humidity.

2 RCC Reporting. In addition to the individual calibration results discussed below, RCC generates a time-series plot of the direct-normal, diffuse-sky irradiance, and computed reference global irradiance, shown in Fig. 8. Time-series plots of *meteorological observations* (estimated atmospheric turbidity, relative humidity, and ambient temperature) are reported. Figure 9 is shows typical parameters in the top, middle, and bottom panels, respectively. RCC reports individual pyranometer zenith angle response. Figure 10 is a plot of the zenith angle response for an Eppley PSP. There is not a *typical* response curve for various makes and models of pyranometers.

Our previous version of RCC computes the mean response with each of ten zenith angle bins, each 9 deg wide, from 0 deg to 90 deg and reports the results, as shown in Table 1. In the new version, we will use 2 deg bins, with separate morning and afternoon bins, for a total of 45 bins. This will reduce the uncertainty in R_s as a function of z when morning and afternoon responsivities do not overlap.

The mean responsivity in each z -bin is plotted as a horizontal bar, as shown in Fig. 10. The 45 deg–55 deg and cosine weighted composite responsivities are plotted as horizontal lines spanning the total zenith angle range. The 45 deg–55 deg bin represents an average responsivity for isotropic sky conditions. The *composite* result is computed as the average of all responsivities weighted by $\cos(z)$. Data can be collected using any of these responsivities; however, the most accurate determination of the total



BORCAL 2000–01 Meteorological Observations

Fig. 9 Typical meteorological data for RCC data collection. Aerosol optical depth or turbidity (top), relative humidity (middle), and ambient temperature (bottom)

global irradiance by a pyranometer is accomplished by using the responsivity as a function of zenith (incidence) angle of the direct beam.

RCC Uncertainty

Using a more accurate computation of solar zenith angles [25,26] and measurement of diffuse-sky irradiance [8], required revision of our estimates of uncertainty for earlier BORCAL procedures and instrumentation. Our *base uncertainty* of 1.3% used previously for the reference irradiance calculation for pyranometers is now reduced by a factor of about 2. A detailed uncertainty analysis and new prescription for computing the uncertainty for subsequent BORCAL events are described below.

1 Data Acquisition. The RCC data logger is a Fluke Helios Plus 2287A, with a high-performance analog-to-digital (A/D) converter, and isothermal voltage input cards. One-year accuracy on the DC voltage range used (± 64 mV) is 0.03% of reading $+9$ microvolts (μV) [27]. For a nominal 10 mV ($=10,000 \mu\text{V}$) thermopile pyranometer signal, this amounts to $9+3=12 \mu\text{V}/10000 \mu\text{V}$, or 0.12% for data logger contributions to measurement uncertainty.

2 Transfer of World Radiometric Reference (WRR). Every five years (since 1980), WRR is transferred with an uncertainty of 0.3% from the World Standard Group (WSG) of absolute cavity radiometers to an NREL reference group of cavity radiometers at the World Radiation Center (WRC) at Davos, Switzerland. NREL has documented the transfer process in [14]. NREL transfers the WRR to working reference cavity radiometers during *NREL Pyrheliometer Comparisons* [28]. Root-sum-squaring the

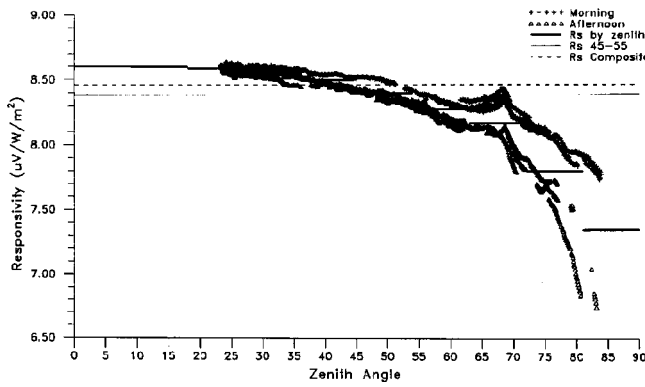


Fig. 10 Pyranometer cosine response curve generated by RCC. Morning data is top leg, afternoon data the bottom leg. Horizontal bars are mean responsivity in zenith angle ranges spanned by the bars.

0.3% uncertainty in WRR from the reference cavity and 0.2% random variation in the transfer of WRR to the working cavity results in the overall uncertainty in direct-beam irradiance of 0.35%. The correction factor to reduce the working cavity irradiance to WWR is $1.0002 \pm 0.35\%$.

3 Zenith Angle Computation. There is uncertainty in the solar zenith angle and $\cos(z)$. This computation depends on knowledge of the latitude, longitude, local standard time, solar equation of time and solar declination [29]. Our BORCAL calibration platform location is known to within 0.0001° , using Global Positioning System (GPS) measurements. RCC software uses GPS time codes to set the time to ± 1 second. The Michalsky algorithm [25,26] is used to compute z within 0.01° . For z less than 75° , the uncertainty in $\cos(z)$ is less than 0.06%. For z greater than 75° , an atmospheric refraction correction [30] is applied to compute an effective zenith angle to an accuracy of 0.02° . The resulting 0.03° uncertainty in $z = 85^\circ$ produces a 0.6% uncertainty in $\cos(z)$, growing to 3% at $z = 89^\circ$.

4 Reference Diffuse-sky Irradiance. The RCC reference diffuse irradiance is the mean of two pyranometers shaded by tracking disks. Whether black-and-white (8–48) or all-black (PSP) detectors are used, uncertainty in the reference diffuse is $\pm 2.5\%$ of reading (due to uncertainty in the R_s) plus W_{off} , where W_{off} is a thermal offset in watts per square meter. W_{off} for PSPs at the NREL site has been characterized to be $-15 \text{ W/m}^2 \pm 5 \text{ W/m}^2$. Thermal offset in a black-and-white (model 8–48) pyranometer is no more than -2 W/m^2 , but the uncertainty in determining the mean of the 3 azimuthal responsivities at 45° is still on the order of 2.5% for both types of pyranometer. NREL uses the mean of two shade/unshade, calibrated black-and-white (model 8–48) pyranometers for RCC diffuse reference irradiance measurements.

5 Total Uncertainty Calculation. Summing the uncertainty from the data logger (0.12%), WRR and transfer of WRR (0.35%), and $\cos(z)$ (0.06% for $z < 75^\circ$), uncertainty in the computation of the direct beam vertical component, U_{dn} , is 0.53%. Since the uncertainty for each individual responsivity, R_s , is a function of the zenith angle and the magnitude of the [black-and-white, 8–48 detector] diffuse irradiance, RCC computes the uncertainty, U_i , for each individual R_s using:

$$U_{dn} = 0.53\% \quad (3)$$

$$U_z = 100 \cdot \frac{(\cos(z) - \cos(z + 0.03^\circ))}{\cos(z)} \% \quad (4)$$

Table 1 RCC report of mean pyranometer responsivity within zenith angle bins

Bin	R_s	Unc	Pct
45–55	8.262	0.18	2.2
Composite	8.328	0.45	5.4
Zen 00–09	8.406	0.18	2.1
Zen 09–18	8.408	0.17	2.0
Zen 18–27	8.387	0.18	2.1
Zen 27–36	8.353	0.19	2.2
Zen 36–45	8.314	0.20	2.4
Zen 45–54	8.265	0.18	2.2
Zen 54–63	8.214	0.18	2.2
Zen 63–72	8.208	0.25	3.0
Zen 72–81	8.118	0.28	3.4
Zen 81–90	7.972	0.27	3.3

Bin=Zenith angle bin identifier

R_s =Mean responsivity within bin (both morning and afternoon data) $\mu\text{V/W/m}^2$

Unc=Uncertainty in units of R_s ($\mu\text{V/W/m}^2$)

Pct=Uncertainty as a percent of mean responsivity (percent)

45–55=Bin for computing responsivity under isotropic conditions

Composite= $\cos(z)$ weighted mean responsivity

$$U_{df} = 100 \cdot \frac{(2.0 + 0.025 \cdot I_{df})}{(I_{dn} \cdot \cos(z) + I_{df})} \% \quad (5)$$

$$U_i = \sqrt{U_{dn}^2 + U_z^2 + U_{df}^2} \% \quad (6)$$

U_z is the percent uncertainty in the $\cos(z)$ term for $z > 75^\circ$, U_{df} is the uncertainty in the diffuse sky irradiance.

After each of the ten zenith-angle bins is completed, the mean responsivity, R_s , for the ten (9° wide) zenith-angle bins is computed. The total uncertainty for the mean responsivity, U_{R_s} , in each bin is the root-sum-square of the mean of the U_i , and one-half of the range $R = (\text{maximum} - \text{minimum})$, as a percentage of the mean R_s for the bin, as shown in Eq. (7).

$$U_{R_s} = \sqrt{\bar{U}_i^2 + \left(100 \cdot 0.5 \cdot \frac{R}{\bar{R}_s}\right)^2} \quad (7)$$

The range term reflects the fact that morning and afternoon responsivities may not overlap, as shown in Fig. 10.

For the uncertainty in the determination of the responsivities of pyrheliometers, the sum of data-logger and absolute-cavity thermometer uncertainty is 0.47% (no zenith-angle or diffuse term). After the mean responsivity, R_s , and the range, R , (maximum – minimum) as a percentage of the mean are computed, the uncertainty in R_s , U_{R_s} is computed as

$$U_{R_s} = \sqrt{(0.47)^2 + \left(100 \cdot \frac{R}{\bar{R}_s}\right)^2} \quad (8)$$

Correcting Zenith Angle Response

The most accurate determination of the total global irradiance is computed from pyrheliometer direct beam and a well calibrated shaded black-and-white pyranometer diffuse measurements. RCC derived Pyranometer zenith angle response corrections for $z < 70^\circ$ are less than 3% of reading; and they increase to about 15% of reading for $z > 80^\circ$.

Figure 11 shows applying RCC zenith angle bin corrections reduces pyranometer error in the clear sky global irradiance from 40 W/m^2 to less than 15 W/m^2 , or 37%.

Irradiance levels under cloudy skies are lower than the irradiances under clear conditions. Under partly cloudy conditions, the direct beam is either blocked or unblocked. Zenith-angle corrections results in much smaller absolute W/m^2 corrections under cloudy conditions. We have applied corrections uniformly under cloudy, clear, and partly cloudy conditions when the direct beam is both absent and present and noted very small corrections (less

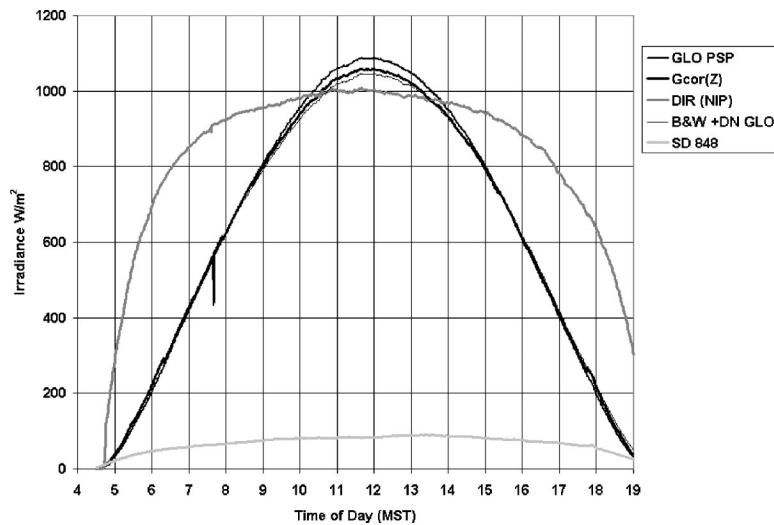


Fig. 11 Top curve (GLO PSP) is measured global irradiance using a single responsivity. The next curve down (thick black line, Gcor[Z]) is the corrected data using responsivity for the appropriate zenith-angle bin. The third line down (thin gray line, B&W+DN GLO) is the computed irradiance from beam and diffuse.

than 5 W/m^2) when the direct beam is absent, and 30 W/m^2 to 40 W/m^2 corrections in global irradiance measurements when the direct beam is present.

Conclusions

The components of uncertainty in responsivity for an all-black pyranometer and black-and-white pyranometer clear sky diffuse reference irradiance are 2.25% and 0.45%, respectively. The improved diffuse measurement, using two black-and-white pyranometers with azimuth averaged responsivities for the reference diffuse irradiance is a factor of 5 smaller.

Improvements in RCC/BORCAL operations and procedures have the following specific impacts:

1. Clear-sky total global solar radiation data from pyranometers calibrated at NREL before March 2000 are about 2.5% to 3% (of reading, 25 W/m^2 to 30 W/m^2 at 1-sun of 1000 W/m^2) too low.
2. Absolute uncertainty in responsivities of pyranometers and pyrhemometers has been reduced by more than 15%.
3. Using black-and-white pyranometers for diffuse reference irradiance improves the absolute accuracy of total global pyranometer measurements by 15 W/m^2 – 20 W/m^2 at NREL.
4. Total global pyranometer measurements based on component summation technique with an all-black pyranometer for diffuse-sky measurements have an inherent negative bias (about 15 W/m^2 at NREL) built into the derived responsivity, and hence, in the measured data.
5. All-black pyranometers calibrated with component summation (using black-and-white diffuse reference) and used to measure diffuse-sky radiation, will still have inherent negative site dependent (15 W/m^2 at NREL) bias error in the field.

References

- [1] Myers, D. R., 1988, "Uncertainty Analysis for Thermopile Pyranometer and Pyrhemometer Calibrations Performed by SERI," Solar Energy Research Institute SERI/TR-215-3294.
- [2] Myers, D. R., Emery, K. A., and Stoffel, T. L., 1989, "Uncertainty Estimates for Global Solar Irradiance Measurements Used to Evaluate PV Device Performance," *Sol. Cells*, **7**, pp. 455–464.
- [3] Myers, D. R., 1989, "Application of a Standard Method of Uncertainty Analysis to Solar Radiometer Calibrations," *Solar '89 Technical Papers: Proc. of 1989 Annual Conf.*, American Solar Energy Society, pp. 445–449.

- [4] Myers, D. R., and Stoffel, T. L., 1990, "A Description of the Solar Radiometer Calibration (RADCAL) Process at SERI," *Proc. of 1990 Annual Conf.*, American Solar Energy Society, pp. 171–177.
- [5] NREL, 1997, *RCC Radiometer Calibration and Characterization*, NREL Metrology Manual.
- [6] Dutton, E. G., Michalsky, J. J., Stoffel, T. L., Forgan, B. W., Hickey, J., Nelson, D. W., Alberta, T. L., and Reda, I., "Measurement of Broadband Diffuse Solar Irradiance Using Current Commercial Instrumentation with a Correction for Thermal Offset Errors," *J. Atmos. Ocean. Technol.*, in press.
- [7] Stoffel, T. L., Reda, I., Myers, D. R., Renne, D., Wilcox, S., and Treadwell, J., 2000, "Current Issues in Terrestrial Solar Radiation Instrumentation for Energy, Climate, and Space Applications," *Metrologia*, **37**, pp. 399–402.
- [8] Reda, I., and Myers, D., 1999, "Calculating the Diffuse Responsivity of Solar Pyranometers," NREL Technical Report/TP-560-26483, National Renewable Energy Laboratory.
- [9] Wilcox, S. M., Reda, I., Nelson, D. A., and Webb, C., 1999, "Traceability and Verification of Radiometer Calibrations at the Southern Great Plains Radiometer Calibration Facility," *Proc. of Ninth Annual ARM Science Team Meeting*, N. Burleigh and D. Carrothers (eds.), U.S. Department of Energy, Richland, WA.
- [10] Wilcox, S. M., and Stoffel, T. L., 1998, "Radiometer Calibrations at the ARM Southern Great Plains Radiometer Calibration Facility," in *Proc. of Eighth Annual ARM Science Team Meeting*, N. Burleigh and D. Carrothers (eds.), U.S. Department of Energy, Richland, WA.
- [11] Kendall, J. M., and Berhdahl, C. M., 1970, "Two Blackbody Radiometers of High Accuracy," *Appl. Opt.*, **12**, pp. 1089–1091.
- [12] Wilson, R. C., 1973, "Active Cavity Radiometer," *Appl. Opt.*, **12**, pp. 810–817.
- [13] WMO 1983, *Guide to Meteorological Instruments and Methods of Observation WMO No. 8*, Secretariat of the World Meteorological Organization, Geneva, Switzerland. 9.8, Sec. 9.3.1.1.
- [14] Reda, I., 1996, "Calibration of a Solar Absolute Cavity Radiometer with Traceability to the World Radiometric Reference," 79 pp., NREL Technical Report/TP-463-20619, National Renewable Energy Laboratory.
- [15] ASTM 1997a, "Standard Test Method for Calibration of Pyrhemometers by Comparison to Reference Pyrhemometers," ASTM E-816-95, *1997 Annual Book of ASTM Standards, Vol. 14*, American Society for Testing and Materials, Conshohocken, MA.
- [16] Zerlaut, G. A., 1986, "Solar Radiometry Instrumentation, Calibration, Techniques and Standards," *Sol. Cells*, **18**, pp. 189–203.
- [17] Zerlaut, G. A., 1989, "Solar Radiation Instrumentation," in *Solar Resources*, R. Hulstrom (ed.), MIT Press, Cambridge, MA, pp. 203–208.
- [18] ASTM 1997b, "Standard Method for Calibration of Reference Pyranometers with Axis Vertical by the Shading Method," *ASTM E-913-82*, *1997 Annual Book of ASTM Standards, Vol. 14*, American Society for Testing and Materials, Conshohocken, MA.
- [19] Wardle, D. I., Dahlgren, L., Dehne, K., Liedquist, L., McArthur, L. J. B., Miyake, Y., Motschka, O., Velds, C. A., and Wells, C. V., 1996, "Improved Measurements of Solar Irradiance by Means of Detailed Pyranometer Characterization," International Energy Agency Solar Heating and Cooling Program, Task 9 Report IEA-SHCP-9C-2, National Atmospheric Radiation Center, Atmospheric Environment Service, Downsview, Canada.

- [20] Taylor, B. N., and Kuyatt, C. E., 1993, "Guidelines for Evaluating an Expressing the Uncertainty of NIST Measurement Results," NIST Technical Note 1297, National Institute of Standards and Technology, Gaithersburg, MD.
- [21] Gulbrandsen, A., 1978, "On the Use of Pyranometers in the Study of Spectral Solar Radiation and Atmospheric Aerosols," *J. Appl. Meteorol.*, **17**, pp. 899–904.
- [22] Molineaux, B., Ineichen, P., and O'Neill, N., 1998, "Equivalence of Pyrheliometric and Monochromatic Aerosol Optical Depths at a Single Key Wavelength," *Appl. Opt.*, **37**(30), pp. 7008–7018.
- [23] Myers, D. R., and Maxwell, E. L., 1992, "Hourly Estimates of Precipitable Water for Solar Radiation Models." Burley, S., and Arden, M. E. (eds.), *Solar 92: Proc. of 1992 Annual Conf.*, June 1992, American Solar Energy Society, Boulder, CO, pp. 317–322.
- [24] Maxwell, E. L., and Myers, D. R., 1992, "Daily Estimates of Aerosol Optical Depth for Solar Radiation Models." Burley, S., and Arden, M. E. (eds.), *Solar '92: Proc. of 1992 Annual Conf.*, June 1992, American Solar Energy Society, Boulder, CO, pp. 323–327.
- [25] Michalsky, J., 1988a, "The Astronomical Almanac's Algorithm for Approximate Solar Position (1950–2050)," *Sol. Energy*, **40**(3), pp. 227–235.
- [26] Michalsky, J., 1988b, "ERRATA: The Astronomical Almanac's Algorithm for Approximate Solar Position (1950–2050)," *Sol. Energy*, **41**(1), p. 113.
- [27] John Fluke Mfg. Co., 1990, *Helios Plus 2287A Data Acquisition Front End System Manual Vol 1*.
- [28] Reda, I., Stoffel, T., and Treadwell, J., 1999, NPC1999, "Results of NREL Pyrheliometer Comparisons NPC 1999," NREL Internal Metrology Report.
- [29] Iqbal, M., 1983, *An Introduction to Solar Radiation*, Academic Press, New York, p. 13.
- [30] Zimmerman, J. C., 1981, "Sun Pointing Algorithms and Their Accuracy," SAND81-0761, Experimental Systems Operation Division, 4721, Sandia National Laboratories, Albuquerque, NM.